Desalination and Water Treatment
www.deswater.com

doi: 10.5004/dwt.2017.21630

97 (2017) 304–314
November

TiO_2 and modified TiO_2/Fe on photocatalytic reduction of Hg^{2+} using artificial and solar radiation

A.L.S. Coelho[a], A.F. de Almeida Neto[b], F.F. Ivashita[c], G.G. Lenzi[d,*], L.M.M. Jorge[a], O.A.A. dos Santos[a]

[a]*Universidade Estadual de Maringá, Departamento de Engenharia Química, Av. Colombo 5790, CEP 87020-900, Maringá, Paraná, Brazil*
[b]*Universidade Estadual de Campinas, 500, Albert Einstein Ave, 13083-852, Campinas, São Paulo, Brazil*
[c]*Universidade Estadual de Maringá, Departamento de Física, Av. Colombo 5790, CEP 87020-900, Maringá, Paraná, Brazil*
[d]*Universidade Tecnológica Federal do Paraná, Av. Monteiro Lobato s/n, CEP 84016-210, Ponta Grossa, Paraná, Brazil, Tel. + 55 42 32204800; email: gianeg@utfpr.edu.br*

Received 5 July 2017; Accepted 11 November 2017

ABSTRACT

Mercury is a highly hazardous water contaminant; both organic and inorganic forms are cumulatively and extremely toxic. In this context, this study describes the application of TiO_2-based systems modified with 5, 8, 10 and 15 wt% Fe using the impregnation method for the photocatalytic reduction of Hg^{2+}. Characterization of TiO_2 and synthesized materials was performed by using Brunauer, Emmett and Taller area, pore diameter and pore volume, scanning electron microscopy, point zero charge, X-ray diffraction (XRD), Fourier transform infrared spectroscopy, photoacoustic and Mössbauer spectroscopy. The photocatalytic reduction of Hg^{2+} was performed in batch stirred tank reactor and compound parabolic collector solar photoreactor, in the presence of catalysts, under four different reaction conditions. The process of heterogeneous photocatalysis was studied in the treatment of synthetic wastewater containing mercury chloride ($HgCl_2$) in different reaction conditions. In particular, the influence of oxygen and formic acid was analyzed. The results showed that an addition of 8% to the iron weight improved the performance of the photocatalytic titania in the reduction of Hg^{2+} (artificial radiation). In the presence of this catalyst, and reaction medium containing only mercuric chloride in an aqueous solution containing oxygen, Hg^{2+} was 100% reduced, after 3 h of reaction. However, under solar radiation, the reduction of Hg^{2+} obtained was 67%.

Keywords: Photocatalytic reduction, Mercury, TiO_2/Fe catalyst, Characterization

1. Introduction

Mercury (Hg) and its compounds (e.g., calomel, mercuric chloride and extremely dangerous dimethylmercury) are highly hazardous water contaminants, due to the high toxicity and tendency to bioaccumulate even at very low concentrations. Thus, exposure to these substances is a potential risk to wildlife and human health – especially children and fetuses. The main acute and chronic symptoms caused by inorganic mercury are thirst, inflammation of the mouth, kidney degeneration and tremor [1–4].

The release of mercury into the environment takes place via natural sources, such as through volcanoes and hot spring deposits. However, the main contamination by mercury ions is arising from anthropogenic sources, especially from wastewater industries (e.g., electronics, paper and pulp, chlorine-alkali, paints, pharmaceuticals, oil refineries, etc.) [4,5].

* Corresponding author.

That is why many countries have enacted legislation and regulations with the goal to minimize mercury emissions to air, land and water [6]. In that respect, heterogeneous photocatalysis could be used as an alternative treatment of Hg pollutants in the liquid phase, since it has been reported in many studies that this process results in the complete mineralization of many organic and inorganic pollutants, besides operating at mild conditions of temperature and pressure [7,8].

TiO_2 has been widely applied to photocatalytic reactions, because of its exceptional optical and electronic properties, chemical stability, non-toxicity and low cost [1,9]. Nevertheless, its wide band gap energy (3.2 eV for anatase) means that only 5% of the solar spectrum is used. This point has motivated the development of the new photocatalysts [10–12], in particular for the reduction of metal ions [13–15].

To improve photo-property and extend the light, that is, the adsorption range of titanium dioxide, selective doping with metals can be used in the matrix of this semiconductor. Doping makes a double effect; it can reduce the band gap energy and decrease the electron–hole recombination rate, acting as electron traps. Many works have reported that Fe^{3+} can be considered the most appropriate dopant for TiO_2, because its ionic radius (0.64 Å) is similar to Ti^{4+} (0.68 Å), which induces the incorporation of cation in the lattice structure of TiO_2, reducing the band gap [1,16–20].

Therefore, the aim of this present study is to compare the performance of commercial TiO_2 and modified TiO_2/Fe in photocatalytic reduction of Hg^{2+} on different conditions and reaction systems.

2. Experimental procedure

2.1. Chemicals

The following chemicals were used as precursors for preparation of the Fe-doped TiO_2: (i) titanium(IV) oxide (supplied by Sigma-Aldrich with over 99.9% degree of purity); iron nitrate $Fe(NO_3)_3.9H_2O$ (supplied by Sigma-Aldrich with over 99.9% degree of purity) and (iii) deionized water. Mercury chloride ($HgCl_2$) (supplied by Merck, PA) was employed as the source of pollutant Hg^{2+}. $HgCl_2$, formic acid (HCOOH, ~85%, obtained by Synth) and deionized water were used in the synthesis of aqueous solution of Hg^{2+} (120 mg mL^{-1}), while $HgCl_2$, nitric acid (HNO_3, ~65%) and deionized water were used to prepare standard aqueous solutions of mercury.

2.2. Impregnation catalysts

Different concentrations of Fe-doped TiO_2 (5, 8, 10 or 15 wt%) were used to prepare photocatalysts by conventional wet impregnation method, according to the following procedure: titanium(IV) oxide was dispersed in deionized water and, to the resulting mixture, iron nitrate ($Fe(NO_3)_3.9H_2O$), previously dissolved in deionized water, was added. The solution was stirred at room temperature until complete homogenization (~12 h). Then, the excess of solvent was removed by drying under low vacuum at 100°C for 3 h.

2.3. Thermal treatment

The pure commercial TiO_2 and prepared photocatalysts were calcined at 400°C for 4 h in the muffle furnace.

2.4. Characterization of the catalysts

2.4.1. X-ray diffraction

The crystallinity was determined by X-ray diffraction (XRD) using a Bruker D8 Advance X-ray diffractometer with a Cu Kα source (λ = 1.5406 Å), at a voltage of 40 kV and current of 35 mA. Scans were made in 2θ range 29°–70° with a step size of 0.01 and step time of 1 min. Thus, the obtained patterns were compared with the diffraction dataset cards from the Joint Committee on Powder Diffraction Standards (JCPDS) [21].

2.4.2. Specific surface area

Textural properties of solids (specific surface area, average pore radius, pore volume and adsorption–desorption isotherms) were determined with a Quantachrome analyzer (Model Nova 1200) using N_2 adsorption at 77 K. Surface areas were calculated using the Brunauer, Emmett and Taller method, while pore and volume distributions were determined by the Barret, Joyner and Halenda method. Prior to the measurements, pure TiO_2 and TiO_2/Fe samples were degassed at 300°C for 6 h.

2.4.3. Fourier transform infrared spectroscopy

The surface structure of the bare and modified TiO_2 was determined using a Bruker Fourier transform infrared (FTIR) spectrometer. Measurements were performed with pellets made using KBr powder as diluent. The FTIR spectrum was collected between the waves at 400 and 4,000 cm^{-1} in the transmission mode.

2.4.4. Point zero charge

The measurements were conducted in a Beckman Coulter Delsa™ Nano Zeta Potentialand Submicron Particle Size Analyzer. The pH ranged from 2 to 11 and the data were analyzed using Particle Analyzer Delsa™ Nano UI software, version 3.73.

2.4.5. Scanning electron microscopy

The morphology of the synthesized materials was analyzed using a scanning electron microscope (SEM; Model MEV Leo 440i) equipped with a tungsten filament, while the qualitative composition of the particles was determined with an energy dispersive detector (EDS 6070).

2.4.6. Photoacoustic spectroscopy

Band gap energies of TiO_2 and Fe-doped TiO_2 powders were determined using the absorbance data obtained from the photoacoustic spectroscopy study following Tauc's relation $[(\alpha.h.\nu) = C\,(h.\nu - E_g)^n]$, where α is the absorption coefficient; h is the Plank's (6.626×10^{-34} J s); ν is frequency of photons; C is a constant; E_g is the average band gap of the material and n is equal to 0.5 (for direct band gap) [22].

2.4.7. Mössbauer spectroscopy

The Mössbauer spectra of iron-doped TiO_2 were collected at room temperature (298 K), in transmission mode, using a

conventional constant-acceleration spectrometer and a ^{57}Co (Rh) source. The velocity scale was calibrated with a α-Fe foil absorber. The spectra were fitted to Lorentzian line using the Normos fitting program.

2.5. Catalytic experiments

The catalytic experiments were carried out in a batch stirred tank reactor (BSTR) and compound parabolic collector (CPC) solar photoreactor described in a previous paper [23,24].

The BSTR system was equipped with a cell, which has an effective volume of 1,000 mL and was used as reaction chamber, a cooling water jacket and a 450 W high pressure mercury lamp (surrounded by a quartz thimble) positioned axially at the center used as UV radiation source. The temperature of the reaction solution was maintained at 20(±2)°C. This device was used in the blank experiments (photolysis and adsorption) and photocatalytic reactions.

Photocatalytic studies were also performed in CPC solar photoreactor, which consisted of six borosilicate glass tubes, with an involute reflective surface of aluminum around each cylindrical tube. The system was operated in a recirculation mode using a 10 L recycle feed tank, and the recycling was performed by aquarium pump. The solar photoreactor was irradiated with solar light in the months of October and December 2015, during summer season, between 10 a.m. and 2 p.m. Catalytic studies were examined at different reaction conditions using a stock solution of Hg^{2+} (120 mg mL^{-1}) in the presence of formic acid (10 mM) and in the presence of oxygen and formic acid. No adjustments of pH solutions of $HgCl_2$ were made, with remaining natural pH conditions. The reaction runs to determine the extent of mercury photolysis, adsorption and photocatalytic were performed for 3 h. (Conditions: (C1) solution of Hg^{2+} (120 mg mL^{-1}); (C2) solution of Hg^{2+} (120 mg mL^{-1}) in the presence of formic acid (10 mM) as hole scavenger; (C3) solution of Hg^{2+} (120 mg mL^{-1}) in the presence of oxygen as electron scavenger and (C4) solution of Hg^{2+} (120 mg mL^{-1}) in the presence of oxygen and formic acid.)

In order to investigate the ability of UV light to remove or reduce Hg^{2+} from water, photolysis experiments were developed with no catalyst under UV irradiation. Photolysis runs were carried out as follows: 500 mL of reaction solution were placed in a BSTR and exposed to UV light in each condition described previously. At regular time intervals, 3 mL aliquot of the suspension were collected. The analysis of residual mercury concentration in the solutions was spectrophotometrically determined by a SpectrAA-10 Plus Varian spectrophotometer.

With the purpose of checking the degree of Hg^{2+} reduction by TiO_2 and TiO_2/Fe catalysts, a series of batch adsorption experiments were performed in the dark in each condition cited previously. Adsorption runs were carried out as follows: typically, each catalyst (1 g L^{-1}) was suspended in a fresh aqueous solution of Hg^{2+}, and the mixture was kept stirred magnetically for all the reaction time. At different intervals of time 3 cm^3 aliquot of the suspension were collected and filtered through a Millipore (0.45 μm) membrane. The final concentration of mercury was determined by spectrophotometric measurements.

The photocatalytic activity of pure TiO_2 and TiO_2/Fe catalysts was evaluated for the reduction of Hg^{2+} under UV (BSTR) and solar (CPC solar photoreactor) light. In a typical BSTR experiment, 500 mL of fresh aqueous solution of $HgCl_2$, in each condition previously described, was taken in a reactor, then catalysts (1 g L^{-1}) were added. The reaction mixture was stirred in dark until the complete homogenization of photocatalyst; after that, the lamp was switched on to initiate the reaction. The mixture was kept stirred magnetically for all the reaction time. At different intervals of time, 3 mL aliquot of the suspension were collected and filtered similarly to the adsorption experiments. Solar light photocatalytic experiments were carried out the same way as describe for the BSTR analysis, differing in volume of solution used 6,000 mL.

3. Experimental results

Fig. 1 shows XRD patterns of the precursor TiO_2 and samples with different loading of iron. Only crystalline anatase phase (2θ = 25.32°, 36.95°, 37.81°, 38.58°, 48.04°, 53.9°, 55.07°, 62.13°, 62.7° and 68.77°) is identified for pure TiO_2 and powders with 5% and 8% of Fe. Although when increasing the iron-loading for 10 and 15 wt%, the results indicate the coexistence of anatase and hematite (2θ = 24.36°, 33.31°, 35.86°, 40.98°, 49.62°, 57.60° and 64°) phases [21], which is in line with previous observations [22]. With the increase of concentration of Fe ions, the sample patterns showed no difference of anatase peaks, indicating that TiO_2 particles present similar size [25,26].

FTIR spectra (Fig. 2) of the bare TiO_2 and materials produced were performed to investigate the bonding configuration of catalysts. The spectral features of all samples are quite similar. The wavenumber at 3,400–3,600 cm^{-1} is due to the stretching vibration mode of the O–H groups, while the bands in the low energy region of spectrum (<1,000 cm^{-1}), 653–550 and 495–436 cm^{-1}, are ascribed to Ti–O and Ti–O–Ti bending vibrations, respectively [27,28]. In FTIR analysis there is no band designated as Fe^{3+} vibration, thus results could indicate

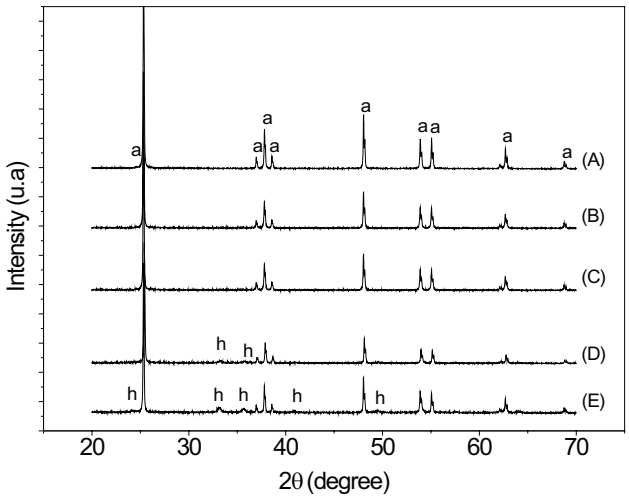

Fig. 1. XRD spectra of the TiO_2/Fe powders: (A) TiO_2; (B) TiO_2 5 wt% Fe; (C) TiO_2 8 wt% Fe; (D) TiO_2 10 wt% Fe and (E) TiO_2 15 wt% Fe. (a) Anatase phase and (h) hematite phase.

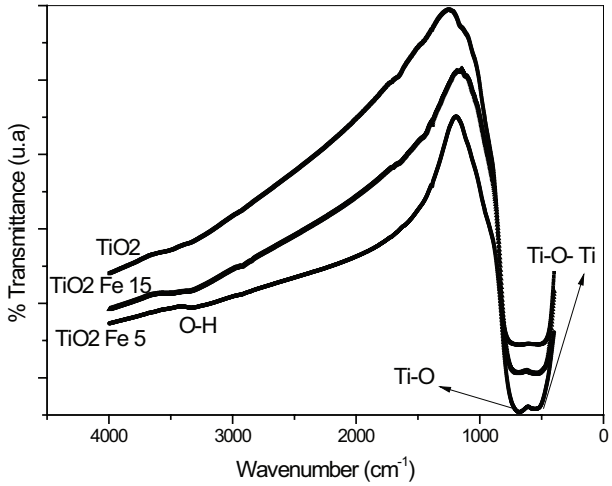

Fig. 2. FTIR spectra of TiO_2 and TiO_2/Fe (with 5 and 15 wt% Fe) powders.

that the dopant (Fe) is incorporated in theTiO_2 lattice or another structure.

The SEM images in Fig. 3 indicate that all the samples are formed by agglomerates of very irregular shape and dimension, regardless of iron loading. The Mössbauer spectra of TiO_2/Fe catalysts are demonstrated in Fig. 4, while the hyperfine parameters are summarized in Table 1.

Only a doublet can be seen in the spectrum for TiO_2/Fe5 and TiO_2/Fe8 samples. The other two samples showed spectra (TiO_2/Fe10 and TiO_2/Fe15) composed of a fit doublet and additionally sextet, which rapidly increases with the Fe content [17,28]. According to data available in the literature [30,31], the values corresponding to IS = 0.37 mm s^{-1}, Qua = –0.21 mm s^{-1} and Bhf = 51 T can be used to identify hematite (α-Fe_2O_3) in synthetic or natural samples [24]. The sextet present in the TiO_2/Fe15 sample is more intensive than the doublet, with the spectral area of the hematite corresponding to 95.4% of the current Fe, implying that the increase in the concentration of Fe induces the formation of hematite agglomerates, disfavoring the insertion of Fe^{3+} in the crystalline structure of TiO_2. Once again, Fe^{3+} is inserted in a compound with a defined geometric structure, justifying the absence of bands corresponding to Fe^{3+} vibration in FTIR analyses.

The values of isomer shift and quadrupole splitting obtained for all doublet spectrums are characteristic of octahedral Fe^{3+} charge state [29] with possible substitutional Fe^{3+} inside anatase lattice. This implies that some Fe ions are incorporated into the TiO_2 lattice, while others are aggregated to hematite [28].

Table 2 summarizes the surface textural properties and bandgap energy for the prepared catalysts (TiO_2/Fe) compared with commercial TiO_2. It can be seen that the addition of Fe, in general, has led to an increase in the specific surface areas, when compared with the pure oxide, except in the sample containing 5 wt% Fe. However, specifically for the catalyst containing 15 wt% Fe, a decrease of textural properties was noted. The bandgap energy (E_g) of undoped TiO_2 sample is 3.22 eV, as reported in the literature [1,16] for anatase phase. For TiO_2/Fe catalysts, a decrease of E_g was observed

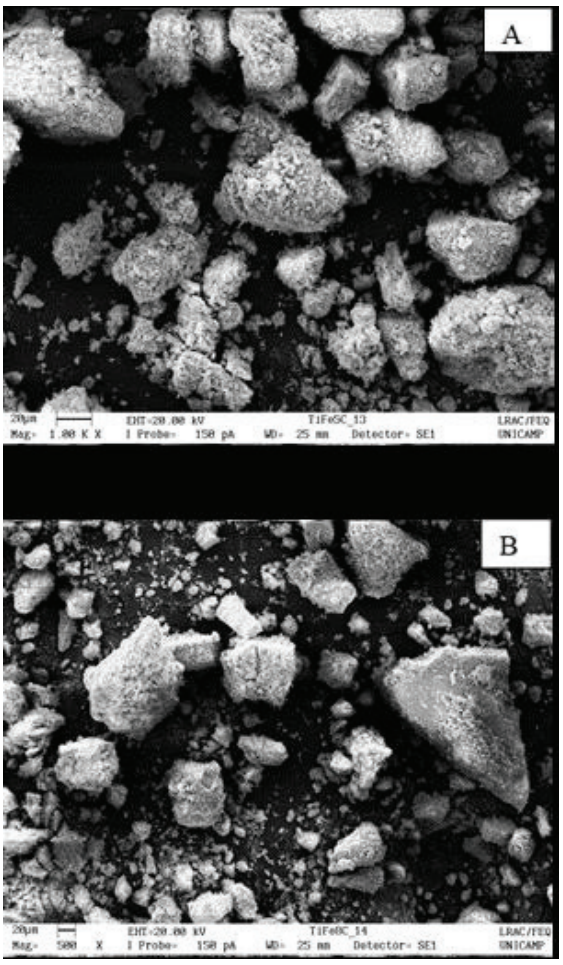

Fig. 3. SEM images of TiO_2/Fe powders: (A) 5 wt% Fe and (B) 8 wt% Fe.

with the increase of Fe content, which can be attributed to the effects of the Fe doping, in accordance with results found by Mössbauer.

The N_2 adsorption–desorption isotherms exhibited similar behavior for TiO_2 and TiO_2/Fe powders (Fig. 5). The plots of the catalysts can be ascribed to type II isotherms according to the IUPAC classification, with most of the samples having mesoporous pores (~50 nm).

The surface charge properties of the photocatalyst were evaluated by point zero charge (PZC) measurements. According to the results, commercial TiO_2 shows pH_{PZC} of 6.0, which agrees with what has been reported in other studies [32,33]. The influence of iron loading upon pH_{PZC} was observed just after thermal treatment. Before calcination, the TiO_2/Fe15, for example, shows pH_{PZC} of 5.8 quite similar with the result for pure semiconductor; after calcination, this value decreased to 4.4.

3.1. Catalytic experiments results

Figs. 6 and 7 show the results of the photolysis and adsorption experiments, respectively. It is possible to observe that the isolated use of UV light and catalysts are not able to completely reduce Hg^{2+} present in the solution. The data of

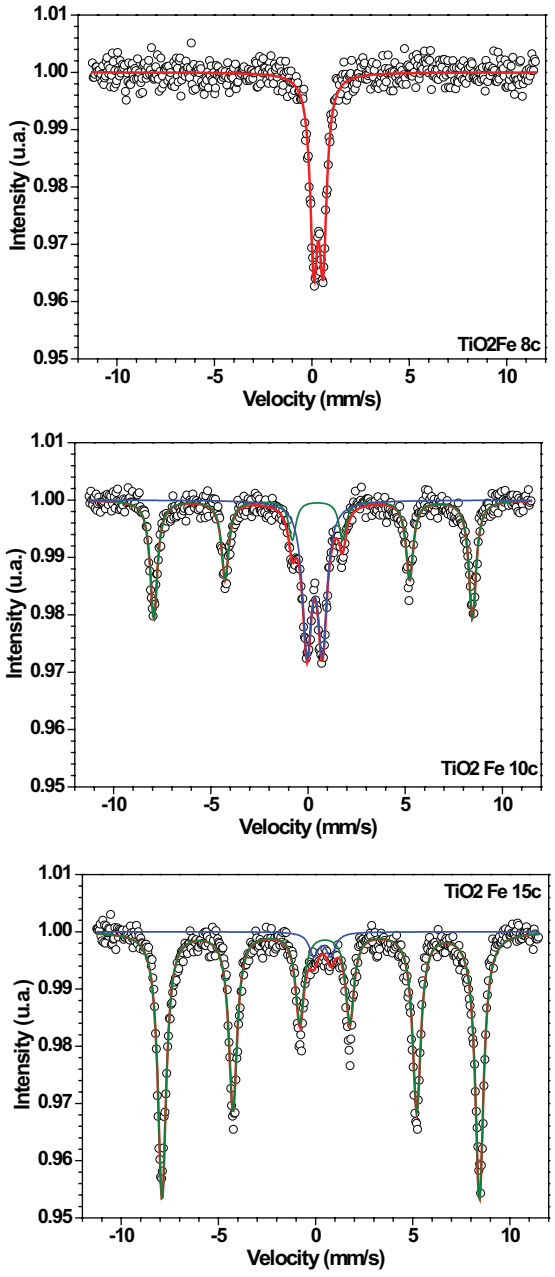

Fig. 4. Mössbauer spectra of TiO_2/Fe samples with different Fe concentration.

Table 2
Specific area (S_g), average pore radius (R_p), pore volume (V) and band gap energy (E_g) for commercial TiO_2 and TiO_2/Fe catalysts

Catalyst	S_g ($m^2\ g^{-1}$)	R_p (Å)	V ($cm^3\ g^{-1}$)	E_g (eV)
TiO_2	10	22	0.001	3.22
TiO_2Fe5	7	13	0.0003	1.73
TiO_2Fe8	14	20	0.0092	1.65
TiO_2Fe10	18	25	0.0166	1.63
TiO_2Fe15	15	20	0.0106	1.63

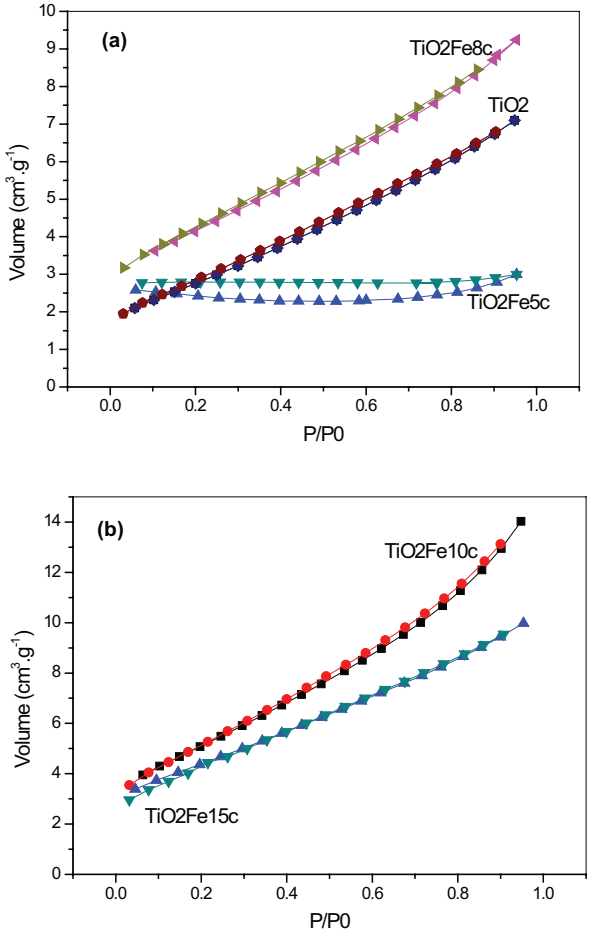

Fig. 5. N_2 adsorption–desorption isotherm of TiO_2 and TiO_2/Fe samples with different Fe concentration.

Table 1
Results of Mössbauer spectra for TiO_2 powders

Sample	Spectrum	T (K)	IS (mm s^{-1}) ±0.01	Qua (mm s^{-1}) ±0.01	Bhf (T)	A (%)
TiO_2Fe5	Doublet	300	0.35	0.8	–	100
TiO_2Fe8	Doublet	300	0.34	0.47	–	100
TiO_2Fe10	Doublet	300	0.35	0.79	–	43
	Sextet		0.37	–0.22	50.8	57
TiO_2Fe15	Doublet	300	0.35	0.86	–	4.6
	Sextet		0.37	–0.21	50.6	95.4

Note: Temperature (T), isomer shifts (IS), quadrupole splitting (Qua), magnetic hyperfine field (Bhf) and absorption area (A).

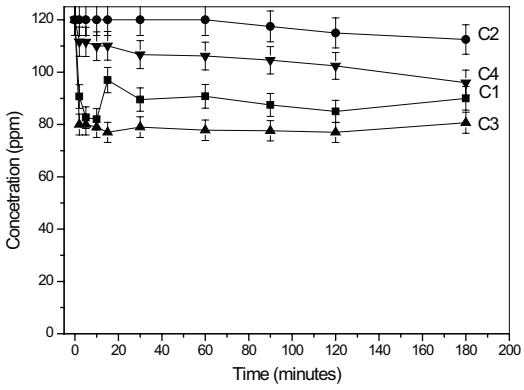

Fig. 6. Concentration of Hg^{2+} for UV light by photolysis test.

photolysis show that, at the end of the reaction time, approximately 33.4%, 22.92%, 18.75% and 6.25% of Hg^{2+} was removed in C3, C1, C4 and C2 conditions, respectively. Adsorption of Hg^{2+} in all experimental conditions here considered showed percentages of mercury reduction between 1.4% and 35.84%. For both studies, no equilibrium condition was found.

Fig. 8 shows the photocatalytic activity over TiO_2 and TiO_2/Fe powders, for batch systems. The batch photocatalysis test conducted with pure commercial TiO_2, showed best results in C1 condition, with residual concentration and percentage of reduction of approximately 16.1 ppm and 86.6%, respectively. The C2, C3 and C4 reaction conditions showed percentage of reduction of 73.6%, 74% and 75.86%, respectively.

The catalyst containing 5 wt% Fe showed better performance in reaction condition 2, with Hg^{2+} reduction of

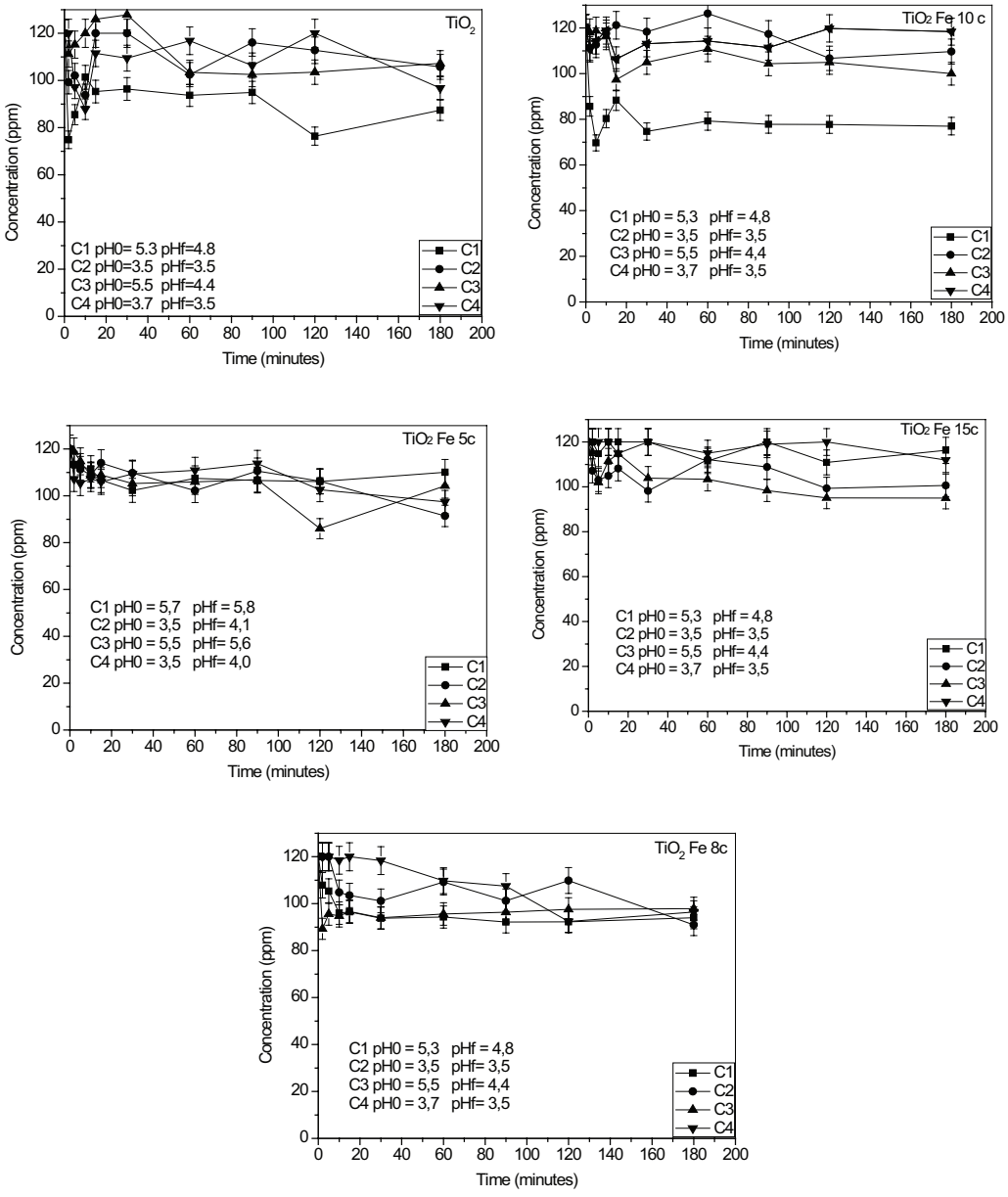

Fig. 7. Concentration of Hg^{2+} for TiO_2 and TiO_2/Fe – adsorption test (pH_0 – initial pH; pH_f – final pH).

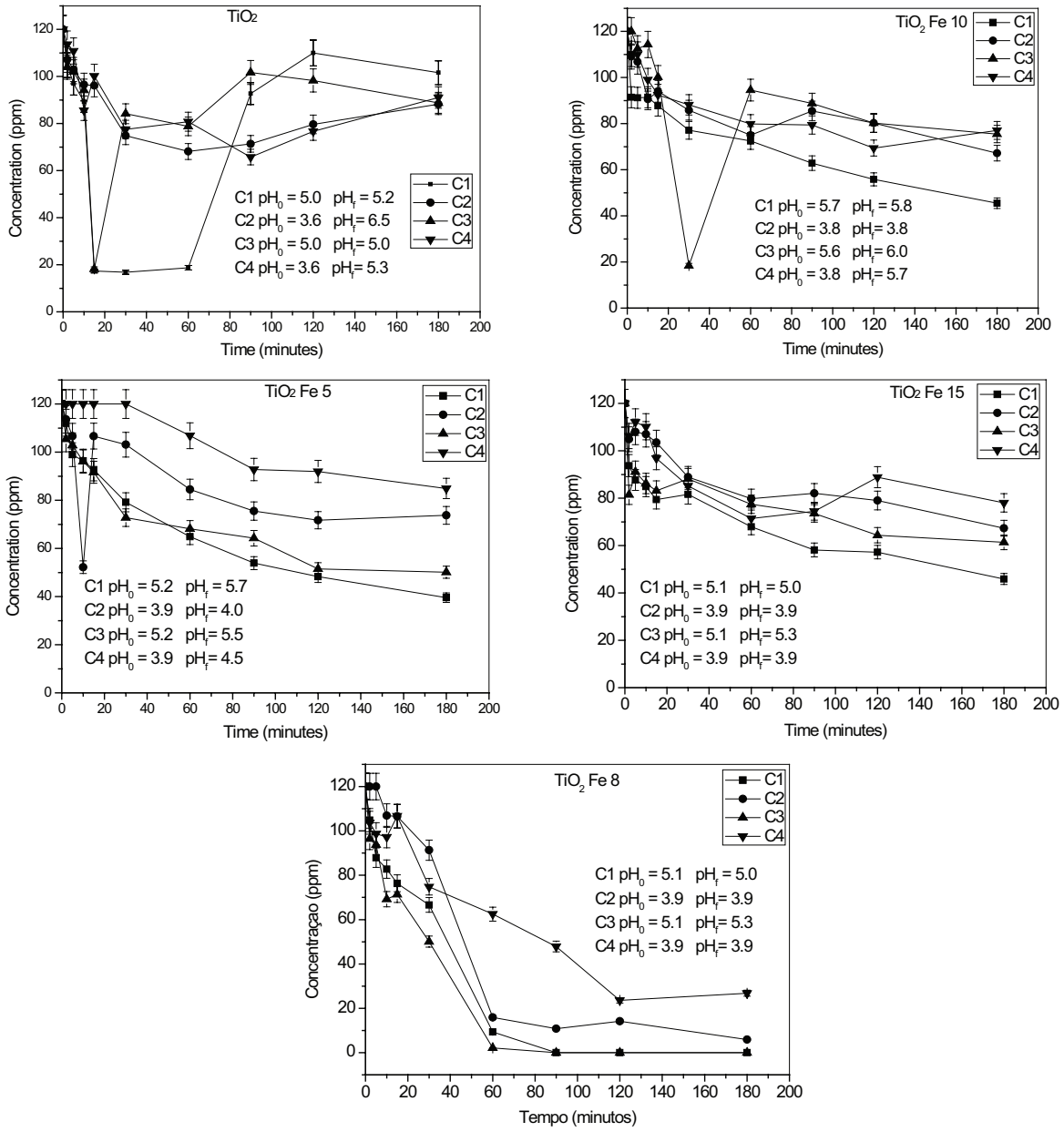

Fig. 8. Concentration of Hg^{2+} for TiO_2 and TiO_2/Fe – photocatalysis batch system test (pH_0 – initial pH; pH_f – final pH).

approximately 56%. A reduction of about 80% Hg^{2+} in the reaction medium containing $HgCl_2$ solution and formic acid (C2) was found for the TiO_2/Fe10 photocatalyst. Whereas, for TiO_2/Fe15, the best result was obtained for pure solution of $HgCl_2$, with removal percentage of about 60%.

Regarding the catalyst TiO_2/Fe8 in batch reactor experiments, after 3 h of reaction, mercury was completely reduced – within the limits of detection of the atomic absorption equipment employed in reading – when the reaction was performed with the aqueous solution containing only mercury chloride (C1) and the solution containing mercury chloride and oxygen as hole scavenger (C3). For the reaction medium comprising the aqueous solution containing the mercury chloride and formic acid as hole scavenger (C2), the percentage reduction was 95%; whereas, for the solution containing mercuric chloride, formic acid and oxygen (C4), this value was 77.7%. As shown in Fig. 9, for solar reactor experiments, the TiO_2/Fe8 catalyst showed a good level of reduction (70.6%) when the reaction was performed with the aqueous solution containing only mercury chloride (C1), with little or no efficiency in other conditions.

Thus, under UV radiation, the catalysts with 8 wt% of Fe are more efficient in reducing Hg^{2+} than pure TiO_2 and other catalysts with metallic charge. This indicates some influence of the dopant concentration. Therefore, at the end of the photocatalytic reaction for TiO_2/Fe8 catalyst, an XRD analysis of the filtered solids in order to reveal the type of deposition mercury compound on the semiconductor surface (Fig. 10). Every XDR pattern exhibits peaks corresponding to calomel

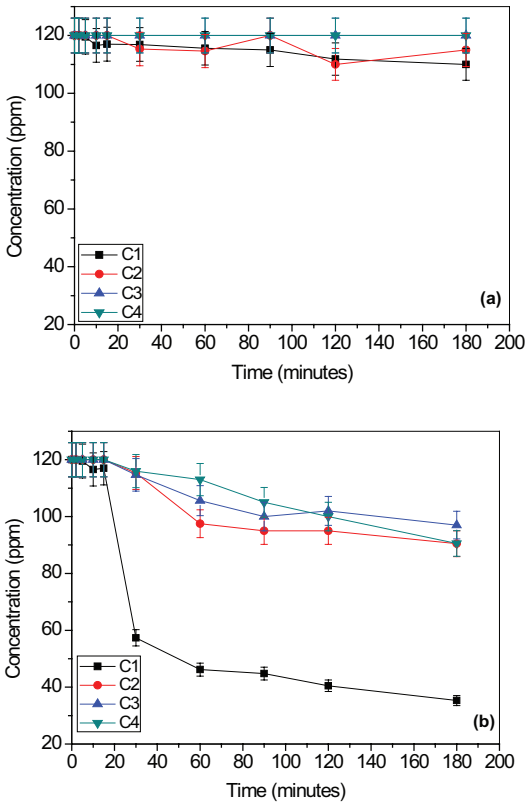

Fig. 9. Concentration of Hg^{2+} for (A) TiO_2 and (B) TiO_2 8 wt% Fe – photocatalysis solar system test.

(Hg_2Cl_2). For C1 condition, six strong peaks (2θ = 21.31°, 28.3°, 33.17°, 40.6°, 43.86° and 46.8°) were observed, with similar results obtained for C3 condition, though peaks became smaller. In C2 and C4 reaction conditions, the amount of calomel peaks was less intense compared with other XDR results.

4. Discussion

4.1. Catalyst characterization

The results found clearly indicate that the incorporation of different amounts of iron into TiO_2, by the procedure described before, leads to considerable matrix differences in commercial TiO_2 photocatalyst.

XRD and Mössbauer studies of the samples revealed that TiO_2/Fe with iron percentage of 5 and 8 wt% exhibits doping features, with iron ions fully incorporated into TiO_2 lattice. For higher Fe percentage, secondary hematite phase was observed to be precipitated, which can be attributed to calcination treatment [17,29]. According to Zboril et al. [30], α-Fe_2O_3 is one of the final products of thermal conversion of a variety of iron(II) and iron(III) compounds.

The characterization of textural properties showed that, for TiO_2/Fe5, little reduction has been found for specific surface area (S_g), average pore radius (R_p) and pore volume (V) parameters, when compared with pure TiO_2. This fact may be due to sintering and crystal growth during the calcination process [17,28]. This can be further attributed to the replacement of Fe atoms in the TiO_2 matrix since, under synthetic conditions, Fe^{3+} preferentially enters interstitial position in the anatase lattice. The variation of bond length of the Fe–O and Fe–Ti could cause local distortion [25,29]. Opposite

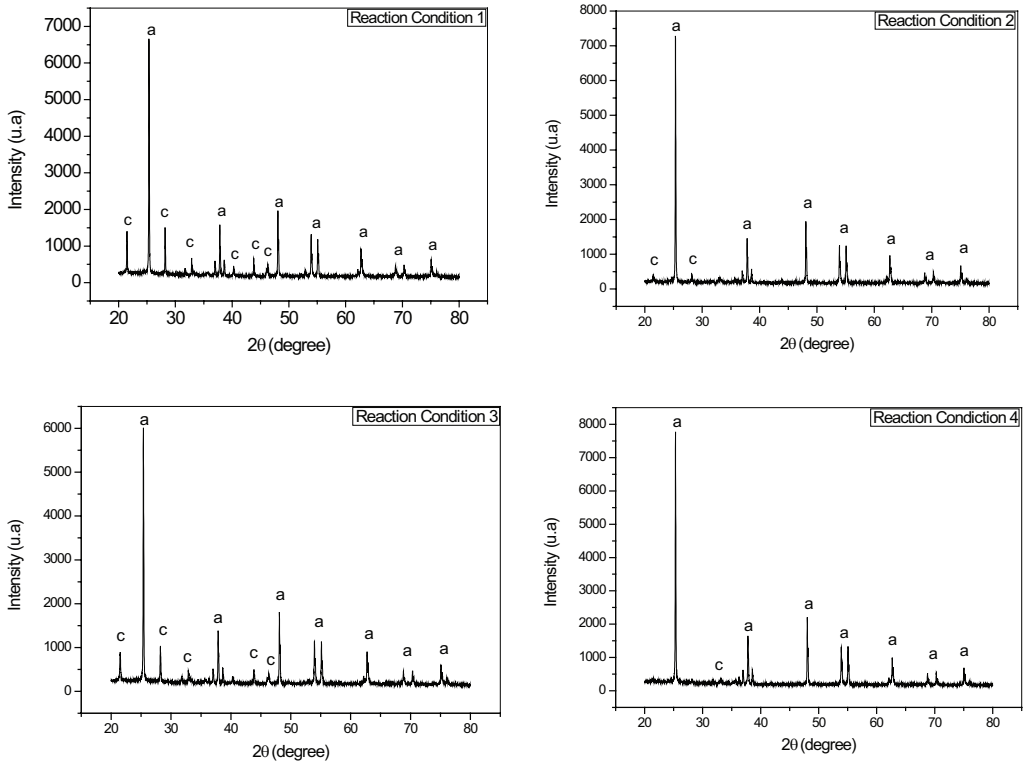

Fig. 10. XRD spectra for TiO_2 8 wt% Fe powder, after photocatalysis reaction in batch system.

behavior was observed for TiO_2/Fe8 photocatalyst, suggesting that a large amount of Fe^{3+} can act as a dispersing agent, preventing TiO_2 agglomeration, and providing a high active surface area of catalyst [34]. The S_g, R_p and V increased with amount of doped iron for 10 wt%, providing possible mixing of the TiO_2 and α-Fe_2O_3 powders. Specifically for the catalyst containing 15 wt% Fe, a decrease of textural properties was observed. The higher percentage of hematite present in this sample has possibly led to particle agglomeration and a blockage of TiO_2 pores [30,32].

Photoacoustic spectroscopy depicts displacement of the bandgap energy by smaller wavelength values than pure TiO_2. For TiO_2/Fe5 and TiO_2/Fe8 values found can be associated with the effect of metal ion dopants [35]. For the samples containing 10 and 15 wt% of iron, the results present two possible analysis: (i) Fe^{3+} ion doping along with the deposition of hematite particles on titania dioxide surface or (ii) formation of heterojunctions semiconductors in mixed oxides. Photocatalysts as TiO_2, ZnO, WO_3, $ZnWO_4$, Bi_2WO_6 and α-Fe_2O_3 have been studied for synthesis of heterojunctions semiconductors. In the case of multiphasic TiO_2 and α-Fe_2O_3, the electrons and holes can be derived from the iron or mixed oxide phase, which extends absorption band in the visible region observed for TiO_2/Fe10 and TiO_2/Fe15 samples [35,36]. Moreover, the distance between the quasi-Fermi level of electrons and the conduction band edge decreases as Fe increases in TiO_2 [22].

No hint of Fe^{3+} was obtained from FTIR results which could be associated with the same vibrations of dopant into anatase and hematite lattice, according to Zhu et al. [25], from the crystal structure of TiO_2 (anatase) and α-Fe_2O_3, both Ti and Fe atoms have six nearest oxygen ions, with Ti in the interstitial sites of octahedrons. This result is consistent with Mössbauer analysis.

Finally, the change in PZC value could be due to alterations by iron doping, since surface sites can also be modified by Fe^{3+} dopant. Therefore, surface properties may be altered, and, consequently, a modification of adsorption properties takes place [35].

4.2. Catalytic experiments discussion

The data present in Fig. 7 show that mercury has a little adsorption affinity for the pure TiO_2 and synthesized photocatalysts. This behavior may be due to the PZC of TiO_2 and TiO_2/Fe powders. Thereby, in acidic medium, the surfaces of photocatalysts become positively charged, making an electrostatic attraction with Hg^{2+} harder [19,35,38,39]. In fact, both charge of photocatalysts surface and speciation of mercury compounds are significantly affected by the solution pH, therefore influencing the process of Hg^{2+} adsorption [2]. According to studies by Aguado et al. [37], the concentration of Hg^{2+} still depends on the semiconductor adsorption ability. For the pure TiO_2, for example, the authors observed that, at concentrations below 2 ppm, mercury is strongly adsorbed on the surface of the titanium, and an opposite behavior was noted for concentrations above 4 ppm.

Regarding photocatalytic experiments conducted under UV radiation, the catalyst containing 8 wt% Fe showed better efficiency in the photocatalytic reduction of Hg^{2+}. However, similar performance was expected for oxide containing 5 wt% Fe since, according to data from Mössbauer spectroscopy, it showed the same doping characteristics. This could be justified by differences in Mössbauer spectroscopy, which quadrupole splitting values are 0.49 and 0.80 mm s^{-1} for TiO_2/Fe 5 and TiO_2/Fe 8, respectively. This has led to a conclusion that Fe^{3+} possibly occupies different locations within the structure of each catalyst. Furthermore, the catalyst 8 wt% Fe has a specific surface area of 14 m^2 g^{-1} and pore volume of 0.0092 cm^3 g^{-1}, while the catalyst 5 wt% Fe has a specific surface area and pore volume of 7 m^2 g^{-1} and 0.0003 cm^3 g^{-1}, respectively. This suggests the possibility of further reduction by the catalyst with 8 wt% of iron when compared with a catalyst containing 5 wt% of iron.

Hung et al. [28] have noted that Fe^{3+} present in the crystalline structure of the catalyst, by doping, can minimize the recombination of electrons and holes by means of the reactions present in Eqs. (1) and (2):

$$Fe^{3+} + e^- \rightarrow Fe^{2+} \quad (1)$$

$$Fe^{3+} + h^+ \rightarrow Fe^{4+} \quad (2)$$

Considering the results obtained for the catalyst TiO_2/Fe8 in reaction condition 1, it is possible to suppose that the Fe^{3+} ions could react with the photogenerated holes, allowing the Hg^{2+} ions to react with electrons, been completely reduced. For the reaction conditions into which formic acid was added, there was the presence of less significant calomel peaks. As previously mentioned, this fact can be associated with higher acidity of the medium as compared with the solution containing only mercuric chloride, which minimizes the potential for the reduction of TiO_2 bands, leading to the formation of different kinds of mercury in the reaction medium. Formic acid influences $CO_2^{h^-}$ metal reduction in two ways: formate can scavenge the photogenerated holes and, the initial oxidation of formate by photogenerated holes and/or hydroxyl radical yields which is strongly reducing $E^0(CO_2^-/CO_2 = -1.8V)$ and can, hence, also take part in the photoreduction process [35].

López-Muñoz et al. [2] reported that, in aqueous acidic conditions, the reduction mechanism of Hg^{2+} is oriented to calomel formation. This equation is in good agreement with the results reported in Fig. 10, which suggest that adsorption equilibrium is really dependent on the surface acidic–basic characteristic of powders.

Regarding the samples of TiO_2/Fe10 and TiO_2/Fe15, due to the presence of a second hematite phase, the system possibly behaves as coupled semiconductors, setting the energy levels of the conduction or valence band to inadequate values for charge transfer to adsorbed substrates [40]. In addition, the α-Fe_2O_3 reduced mobility of charge carriers, promoting a fast recombination rate responsible for the small efficiency of hematite in photocatalytic processes [41].

Therefore, the ideal concentration of dopant, in this case 8 wt%, would make the thickness of space charge layer substantially equal to the light penetration depth [35].

Regarding photocatalytic experiments conducted in solar reactor, the results demonstrate that TiO_2 has little activity under visible light. This result is in fact expected, since the data from photoacoustic spectroscopy show characteristic absorption of TiO_2 at 400 nm. For TiO_2/Fe8 powder, the low effectiveness observed could be related to the fact that the

synthesized material has high weight and it was difficult to keep all the concentration of catalyst in suspension throughout the reaction period. This could lead to the saturation of the catalyst surface due to the high concentration of Hg^{2+} in the solution reaction. Moreover, it was observed that, during reaction time, part of water contained in solution had evaporated, observing condensation in borosilicate tubes. These temperature conditions disfavor the contaminant adsorption on the catalyst surface [39].

5. Conclusions

An 8% addition of iron weight has improved the performance of the photocatalytic titania in the reduction of Hg^{2+}. In the presence of this catalyst, and reaction medium containing only mercuric chloride in an aqueous solution containing oxygen, Hg^{2+} was reduced, after 3 h of reaction. This can be due to the effectiveness of the doping, specific surface area and pore volume of the catalyst. However, under solar radiation, it was not possible, under the conditions studied, to obtain complete reduction of Hg^{2+}. For TiO_2 batch reactor, present in the reaction medium containing only residual mercuric chloride, Hg concentration was approximately 13.4%. In the presence of other reaction mixtures, the percentage of reduction of Hg^{2+} remained around 26%, which was mainly associated with the acidic conditions of the solutions used. In solar reactor, TiO_2 catalyst hardly demonstrated ability to reduce Hg^{2+}. Catalysts 5% Fe/TiO_2, 10% Fe/TiO_2 and 15% Fe/TiO_2 calcined at 400°C were not 100% efficient in the reduction of Hg^{2+}, leading to a partial reduction in all conditions and system reactions in this work.

Acknowledgments

G.G. Lenzi thanks the financial support of the CNPq under Grant No. 302415/2016-5.

References

[1] G.G. Lenzi, C.V.B. Fávero, L.M.S. Colpini, H. Bernabe, M.L. Baesso, S. Specchia, O.A.A. Santos, Photocatalytic reduction of Hg^{2+} on TiO_2 and Ag/TiO_2 prepared by the sol–gel and impregnation methods, Desalination, 270 (2011) 241–247.
[2] M.J. López-Muñoz, J. Aguado, A. Arencibia, R. Pascual, Mercury removal from aqueous solutions of $HgCl_2$ by heterogeneous photocatalysis with TiO_2, Appl. Catal., B, 104 (2011) 220–228.
[3] L.C. Mansur, Review of the use of mercury in historic and current ritualistic and spiritual practices, Environ. Med., 16 (2011) 314–320.
[4] H. Parham, B. Zargar, R. Shiralipour, Fast and efficient removal of mercury from water samples using magnetic iron, J. Hazard. Mater., 205–206 (2012) 94–100.
[5] F. Da Pieve, M. Stankowski, C. Hogan, Electronic structure calculations of mercury mobilization from mineral phases and photocatalytic removal from water and the atmosphere, Sci. Total Environ., 493 (2014) 596–605.
[6] B. Dou, H. Chen, Removal of toxic mercury(II) from aquatic solutions by synthesized TiO_2 nanoparticles, Desalination, 269 (2011) 260–265.
[7] C. Siriwong, N. Wetchakun, B. Inceesungvorn, D. Channei, T. Samerjai, S. Phanichphant, Doped-metal oxide nanoparticles for use as photocatalysts, Prog. Cryst. Growth Charact. Mater., 58 (2012) 145–163.
[8] P.R. Gogate, A.B. Pandit, A review of imperative technologies for wastewater treatment I: oxidation technologies at ambient conditions, Adv. Environ. Res., 8 (2004) 501–555.
[9] S. Rengaraj, X.Z. Li, Enhanced photocatalytic reduction reaction over Bi^{3+}–TiO_2 nanoparticles in presence of formic acid as a hole scavenger, Chemosphere, 66 (2007) 930–938.
[10] H. Gan, G. Zhang, H. Huang, Enhanced visible-light-driven photocatalytic inactivation of *Escherichia coli* by $Bi_2O_2CO_3$/Bi_3NbO_7 composites, J. Hazard. Mater., 250–251 (2013) 131–137.
[11] B.K. Mutuma, G.N. Shao, W.D. Kim, H.T. Kim, Sol–gel synthesis of mesoporous anatase–brookite and anatase–brookite–rutile TiO_2 nanoparticles and their photocatalytic properties, J. Colloid Interface Sci., 442 (2015) 1–7.
[12] Z. Wan, G. Zhang, X. Wu, S. Yin, Novel visible-light-driven Z-scheme $Bi_{12}GeO_{20}$/g-C_3N_4 photocatalyst: oxygen-induced pathway of organic pollutants degradation and proton assisted electron transfer mechanism of Cr(VI) reduction, Appl. Catal., B, 207 (2017) 17–26.
[13] Y. Zhang, F. Zhang, Z. Yang, H. Xue, D.D. Dionysiou, Development of a new efficient visible-light-driven photocatalyst from SnS_2 and polyvinyl chloride, J. Catal., 344 (2016) 692–700.
[14] Y.C. Zhang, L. Yao, G. Zhang, D.D. Dionysiou, J. Li, X. Du, One-step hydrothermal synthesis of high-performance visible-light-driven SnS_2/SnO_2 nanoheterojunction photocatalyst for the reduction of aqueous Cr(VI), Appl. Catal., B, 144 (2014) 730–738.
[15] V.N. Salomone, J.M. Meichtry, M.I. Litter, Heterogeneous photocatalytic removal of U(VI) in the presence of formic acid: U(III) formation, Chem. Eng. J., 270 (2015) 28–35.
[16] J.C. Colmenares, M.A. Aramendía, A. Marinas, J.M. Marinas, F.J. Urbano, Synthesis, characterization and photocatalytic activity of different metal-doped titania systems, Appl. Catal., A, 306 (2006) 120–127.
[17] S. Zhu, T. Shi, W. Liu, S. Wei, Y. Xie, C. Fan, Y. Li, Direct determination of local structure around Fe in anatase TiO_2, Physica B, 396 (2005) 177–180.
[18] R.M. Mohamed, M.A. Salam, Photocatalytic reduction of aqueous mercury(II) using multi-walled carbon nanotubes/Pd-ZnO nanocomposite, Mater. Res. Bull., 50 (2014) 85–90.
[19] Y. Wang, Q. Wang, X. Zhan, F. Wang, M. Safdar, J. He, Visible light driven type II heterostructures and their enhanced photocatalysis properties: a review, Nanoscale, 5 (2013) 8326–8350.
[20] J. Zhu, W. Zheng, B. He, J. Zhang, M. Anpo, Characterization of Fe–TiO_2 photocatalysts synthesized by hydrothermal method and their photocatalytic reactivity for photodegradation of XRG dye diluted in water, J. Mol. Catal. A: Chem., 216 (2004) 35–43.
[21] Joint Committee on Powder Diffraction Standards, International Centre for Diffraction Data, PCPDFWIN v.130, 1997.
[22] I. Ganesh, P.K. Kumar, A.K. Gupta, P.S.C. Sekhar, K. Radha, G. Padmanabham, G. Sundararajan, Preparation and characterization of Fe-doped TiO_2 powders for solar light response and photocatalytic applications, Process. Appl. Ceram., 6 (2012) 21–36.
[23] J.M. Herrmann, C. Guillard, Photocatalytic degradation of pesticides in agricultural used waters, Chemistry, 3 (2000) 417–422.
[24] S. Malato, J. Blanco, A. Vidal, C. Richter, Photocatalysis with solar energy at a pilot-plant scale: an overview, Appl. Catal., B, 37 (2002) 1–15.
[25] S. Zhu, T. Shi, W. Liu, S. Wei, Y. Xie, C. Fan, Y. Li, Direct determination of local structure around Fe in anatase TiO_2, Physica B, 396 (2007) 177–180.
[26] X. Zhang, M. Zhou, L. Lei, Preparation of anatase TiO_2 supported on alumina by different metal organic chemical deposition methods, Appl. Catal., A, 282 (2005) 285–293.
[27] M. Gharagozlou, R. Bayati, Photocatalytic characteristics of single phase Fe-doped anatase TiO_2 nanoparticles sensitized with vitamin B12, Mater. Res. Bull., 61 (2015) 340–347.
[28] W.C. Hung, S.H. Fu, J.J. Tseng, H. Chu, T.H. Ko, Study on photocatalytic degradation of gaseous dichloromethane using pure and iron-doped TiO_2 prepared by the sol–gel method, Chemosphere, 66 (2007) 2142–2151.
[29] R. Janes, L.J. Knightley, C.J. Harding, Structural and spectroscopy studies of iron (III) doped titania powders prepared by sol-gel synthesis and hydrothermal processing, Dyes Pigm., 62 (2004) 199–212.

[30] R. Zboril, M. Mashln, D. Petridis, Iron(III) oxides from thermal processes-synthesis, structural and magnetic properties, Mössbauer spectroscopy characterization, and applications, Chem. Mater., 14 (2002) 969–982.
[31] A.M.L. Costa, B.A. Marinkovic, N.M. Suguihiro, D.J. Smith, M.E. H.M. Da Costa, S. Paciornik, Fe-doped nanostructured titanates synthesized in a single step route, Mater. Charact., 99 (2015) 150–159.
[32] T. Gavriloaiei, D. Gavriloaiei, Determination of surface charge for metal oxides, Geologie, 54 (2008) 11–18.
[33] M. Kosmulski, Compilation of PZC and IEP of sparingly soluble metal oxides and hydroxides from literature, Adv. Colloid Interface Sci., 152 (2009) 14–25.
[34] W. Wang, P. Serp, P. Kalck, J.L. Faria, Photocatalytic degradation of phenol on MWNT and titania composite catalysts prepared by a modified sol-gel method, Appl. Catal., B, 56 (2005) 305–312.
[35] O. Carp, C.L. Huisman, A. Reller, A, Photoinduced reactivity of titanium dioxide, Prog. Solid State Chem., 32 (2004) 33–177.
[36] G. Pecchi, P. Reyes, P. Sanhueza, J. Villaseñor, Photocatalytic degradation of pentachlorophenol on TiO_2 sol-gel catalysts, Chemosphere, 43 (2001) 141–146.
[37] M.A. Aguado, S. Cervera-March, J. Giménez, Continuous photocatalytic treatment of mercury(II) on titania powders. Kinetics and catalyst activity, Chem. Eng. Sci., 50 (1995) 1561–1569.
[38] O. Ercan, A. Aydin, Removal of mercury, antimony, cadmium and lead from aqueous solution using 1,3,5-trithiane as an adsorbent, J. Braz. Chem. Soc., 24 (2013) 865–872.
[39] M.N. Chong, B.J. Jin, C.W.K. Chow, C. Saint, Recent developments in photocatalytic water treatment technology: a review, Water Res., 44 (2010) 2997–3027.
[40] J.A. Navío, G. Colón, M.I. Litter, G.N. Bianco, Synthesis, characterization and photocatalytic properties of iron-doped titania semiconductors prepared from TiO_2, and iron(III) acetylacetonate, J. Mol. Catal. A: Chem., 106 (1996) 267–276.
[41] M.I. Litter, J.A. Navío, Photocatalytic properties of iron-doped titania semiconductors, J. Photochem. Photobiol., A, 98 (1996) 171–181.